

PROCEEDINGS OF SPIE

[SPIDigitalLibrary.org/conference-proceedings-of-spie](https://spiedigitallibrary.org/conference-proceedings-of-spie)

Bayesian retrieval algorithm to detect unresolved point sources in JWST/MIRI spectra using the detector-produced interferometric fringes

Danny Gasman, Ioannis Argyriou, Bart Vandenbussche

Danny Gasman, Ioannis Argyriou, Bart Vandenbussche, "Bayesian retrieval algorithm to detect unresolved point sources in JWST/MIRI spectra using the detector-produced interferometric fringes," Proc. SPIE 12180, Space Telescopes and Instrumentation 2022: Optical, Infrared, and Millimeter Wave, 121803O (27 August 2022); doi: 10.1117/12.2627845

SPIE.

Event: SPIE Astronomical Telescopes + Instrumentation, 2022, Montréal, Québec, Canada

Bayesian retrieval algorithm to detect unresolved point sources in JWST/MIRI spectra using the detector-produced interferometric fringes

Danny Gasman^a, Ioannis Argyriou^a, and Bart Vandenbussche^a

^aInstitute of Astronomy, KU Leuven, Celestijnenlaan 200D, 3001 Leuven, Belgium

ABSTRACT

Similarly to other spectroscopic instruments operating in the infrared wavelength range, the observations of the Mid-Infrared Instrument (MIRI) on-board the James Webb Space Telescope (JWST) are subject to fringing. The different layers in the detectors act as Fabry-Pérot etalons, causing fringes up to 30% in depth. The depth and phase of these detector fringes is not constant for all source geometries on the sky, and depends on the illumination of the MIRI pupil. This means that point sources will show a different fringe pattern from semi-extended sources and extended sources. In fact, it has been found that a smooth change in depth and phase occurs depending on what part of the point spread function (PSF) is sampled. Here, we aim to use the predictable change in fringe pattern to find evidence for the presence of an additional body in what is seemingly a single point source. To do this, we create a forward model of the PSF including fringes and insert this into a Bayesian retrieval loop. The Bayesian loop finds the coordinates on the detector for one or more point sources that best fits the data of two point sources added together. We find that the code is able to identify the along-slice coordinates of the two point sources, but there is less of a dependency on the fringes with the across-slice coordinate. Using commissioning and Cycle 1 data, we will be able to better characterise the fringes, and improve the forward models.

Keywords: interferometric fringes, MIRI MRS, JWST, point source, Bayesian retrieval, infrared spectroscopy, infrared detectors

1. INTRODUCTION

The Mid-Infrared Instrument (MIRI) on-board the James Webb Space Telescope (JWST) allows us to probe the 5 to 28 micron range using its Medium Resolution integral field Spectrometer (MRS).¹ In order to cover the full bandwidth, four spectral channels are mapped onto two detectors. The two Si:As detectors consist of several layers, each with their individual wavelength-dependent refractive properties, acting as Fabry-Pérot etalons. Therefore, incoming light shows destructive and constructive interference with itself, resulting in fringes in the spectral direction. Fringing is not unique to MIRI and has been observed in other spectroscopic instruments operating in the infrared wavelength range, such as the Space Telescope Imaging Spectrograph (STIS) on-board the Hubble Space Telescope.²

The full spectral range of the MRS is divided among four channels, each with three sub-bands, resulting in a total of twelve bands (see Tab. 1). The light is split into the different wavelengths, and dispersed onto two detectors: one includes channels 1 and 2, the other 3 and 4. A detector image is presented in Fig. 1, which shows a point source image in channel 1, and uses channel 2 to explain the coordinate system. For each channel, spatial information is retained due to the integral-field units (IFU), which cut the on-sky image into different slices. Each slice has an across-slice coordinate (β), and changing along-slice coordinates (α) in the detector X-direction; both analogous to on-sky right-ascension (RA) and declination (DEC) coordinates. The Y-direction on the detector corresponds to different wavelengths. Since neighbouring slices on the detector are not neighbouring on-sky, the resulting image is complex and the projection of the point spread function (PSF) on the detector is not straightforward.

The spectral resolution of the MRS allows us to resolve the fringes. The nature of these fringes depends on the spatial extent of the source and local properties of the detector, due to changes in the illumination of the MIRI pupil.^{3,4} For point sources it has been observed that the asymmetric pupil illumination results in a depth

Table 1. Division of wavelength ranges in bands, and other properties.³

Channel	Sub-band	Wavelength range [micron]	Number of slices	Field of view [arcsec]
1	A	4.83–5.82	21	3.46 x 3.72
	B	5.62–6.73		3.46 x 3.72
	C	6.46–7.76		3.41 x 3.72
2	A	7.44–8.90	17	4.16 x 4.76
	B	8.61–10.28		4.16 x 4.76
	C	9.94–11.87		4.12 x 4.76
3	A	11.47–13.67	16	6.00 x 6.24
	B	13.25–15.80		5.96 x 6.24
	C	15.30–18.24		5.91 x 6.24
4	A	17.54–21.10	12	7.14 x 7.87
	B	20.44–24.72		7.06 x 7.87
	C	23.84–28.82		6.99 x 7.87

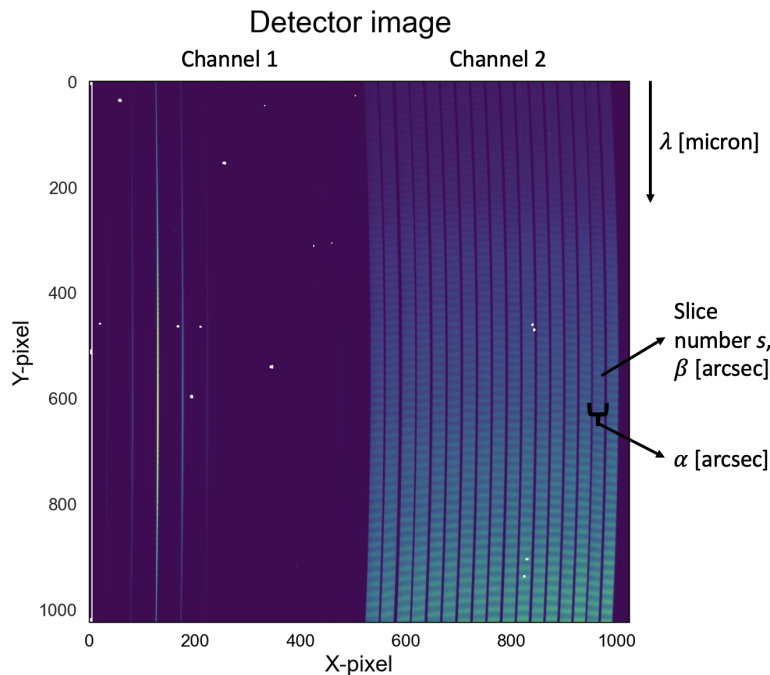


Figure 1. Detector image of bands 1/2A, with a point source in channel 1. The extended illumination in channel 2 is used to visualise the slices, and explain the detector coordinate system.³

and phase change depending on what part of the PSF is sampled.³ The amplitude of the fringes can be as high as 10 to 30% of the spectral baseline, and they therefore directly impact the achievable science with the MIRI MRS. Modelling efforts to calibrate the fringes out of the data show great promise, with residuals of $\sigma \sim 0.5\%$.³

These same models of point source fringes can be used to simulate those of an extended source, by convolving a larger number of modelled point sources. This suggests that a similar approach can be used to model the fringes of other complex scenes, such as crowded fields, or disks. Aside from deriving more accurate fringe corrections, their predictability may prove valuable for another purpose. The presence of an additional unresolved companion will alter the detected fringe pattern compared to a single point source. Using this knowledge, we can exploit the detector and point source fringe properties to create forward models to be used in a Bayesian retrieval framework, to find statistical evidence for the presence of additional close-in bodies in an observation, which otherwise would have been difficult to detect.

A commonly used method in astrophysics to determine a best fit model makes use of Bayesian fitting, while simultaneously finding the evidence of the model being the truth.⁵ However, Bayesian fitting loops can also be

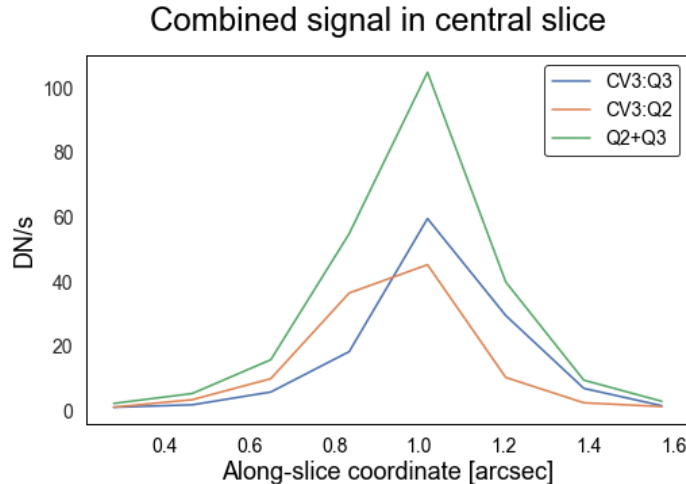


Figure 2. Signal of individual data sets and the two added together, in the central slice.

applied to correct fringes,⁶ and are implemented in the MIRI MRS JWST pipeline.⁷ By comparing the evidence of two assumed models, e.g. one or two point sources, a measure of how strongly a model is favoured over the base can be found: the Bayes factor. The Bayes factor is found by taking the ratio of evidence of one model to another, and significant evidence corresponds to a Bayes factor larger than 5.⁵

We present our approach here, structured as follows. The forward model and Bayesian retrieval loop set-up are described in Sec. 2. The initial results from a retrieval loop can be found in Sec. 3. Finally, we discuss the possibility of adding information from other channels to the method, and summarise our conclusions and recommendations for future work in Secs. 4 and 5.

2. METHODS

2.1 Data to Fit

Two ground test campaigns included point source-like illumination of the detector: the ground cryo-vacuum test campaigns CV2 and CV3, performed in 2014 and 2016 at NASA-GSFC, respectively. These tests included all of the JWST science instruments in the Integrated Science Instrument Module (ISIM), which was kept at operational temperatures during testing. However, point source data from ground tests exist only for band 1A. In this work, we made use of two CV3 data sets that were placed in close proximity to each other: sets Q2 and Q3. By adding the two sets together (see Fig. 2), we can simulate the fringe pattern of two close-in companions. The resulting effect of this addition on the fringes can be found in Fig. 3. The centroids in (α, β) coordinates are $(0.947, -0.302)$ for Q2 and $(1.049, -0.382)$ for Q3. Note that for the fit, all data sets are normalised to limit the search space.

2.2 Forward Model

2.2.1 Projecting the PSF on the detector

The PSF model is provided in a 3D spectral cube with two spatial and one spectral coordinate; the cube model represents a series of super-sampled monochromatic PSFs (the spaxel size is much smaller than the projected size of the detector pixels). The PSF spatial and spectral coordinates are interpolated on a grid with the detector's resolution, and flux values are assigned to the pixels. Due to the way the spatial and spectral coordinates are divided on the detector, the resulting image is the typical MRS detector PSF divided in different slices.

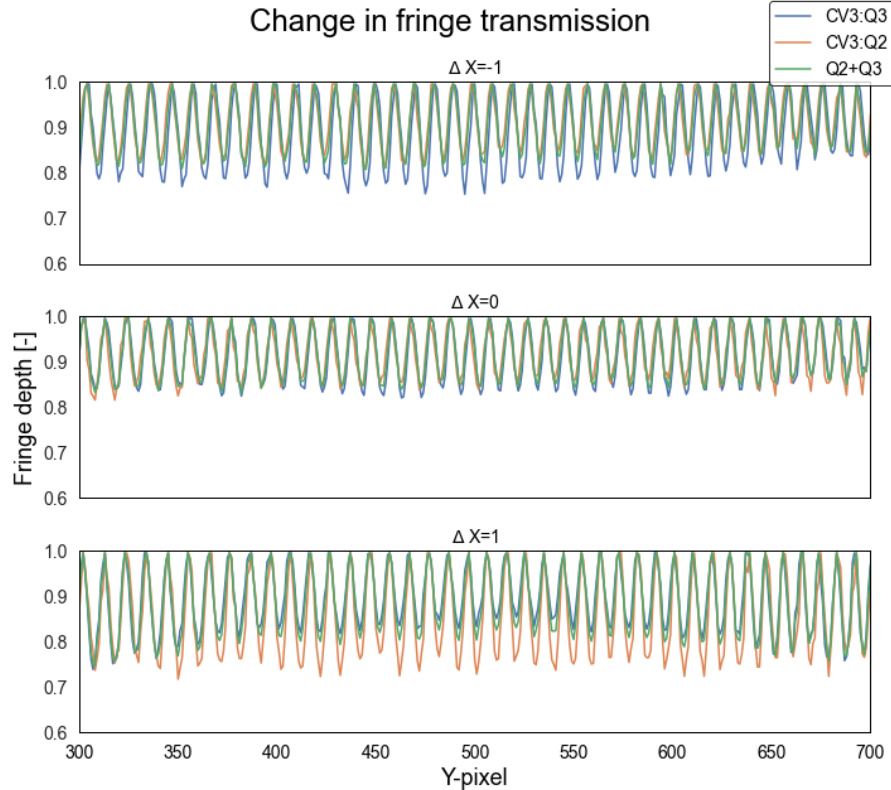


Figure 3. Fringe depth of two separate sets of test data, and the two added together. In the centre of the PSF ($\Delta X = 0$) the fringes are most similar, but as we move away from the peak this is no longer the case.

2.2.2 Modelling the point source fringes

In Fig. 4, the trends of change in fringe depth and phase with along-slice offset from the PSF peak are shown. The different data points indicate different wavelengths, and 17 different point source observations from the CV3 test campaign were combined to produce the trends. This results in a 3-dimensional fourth-order polynomial fit, with dimensions in α , wavelength (λ), and fringe depth or phase. We use these properties in Eq. 1:⁸

$$depth = \left(\frac{1}{T} \sin \left(2\pi D \frac{1}{\lambda} + \phi \right)^2 \right)^{-1}, \quad (1)$$

where T is the transmission depth found previously, D the detector optical thickness, and ϕ the phase from the fit. The clean projected PSF signal is then multiplied by this fringe flat. Due to the lower signal-to-noise ratio (SNR) in the wings of the PSF, only three slices are used in the forward model and consecutive fit: the central slice, and two to the left and right.

2.3 Bayesian Retrieval Loop

The Bayesian retrieval loop is based on the *BayesicFitting*⁹ Python package. We define a new model class, that takes an assumed number of point sources (in this work either one or two) the detector coordinates α and β , and a relative brightness between the two point sources (I). Using these properties, the resulting PSFs are projected onto the detector, after which the previously described fringe forward models are applied to each PSF individually. We examine the one- and two-body cases, and run the NestedSampler with 50 samples, all of which take random values dictated by the uniform priors presented in Tab. 2. A schematic of the flow of the code is shown in Fig. 5.

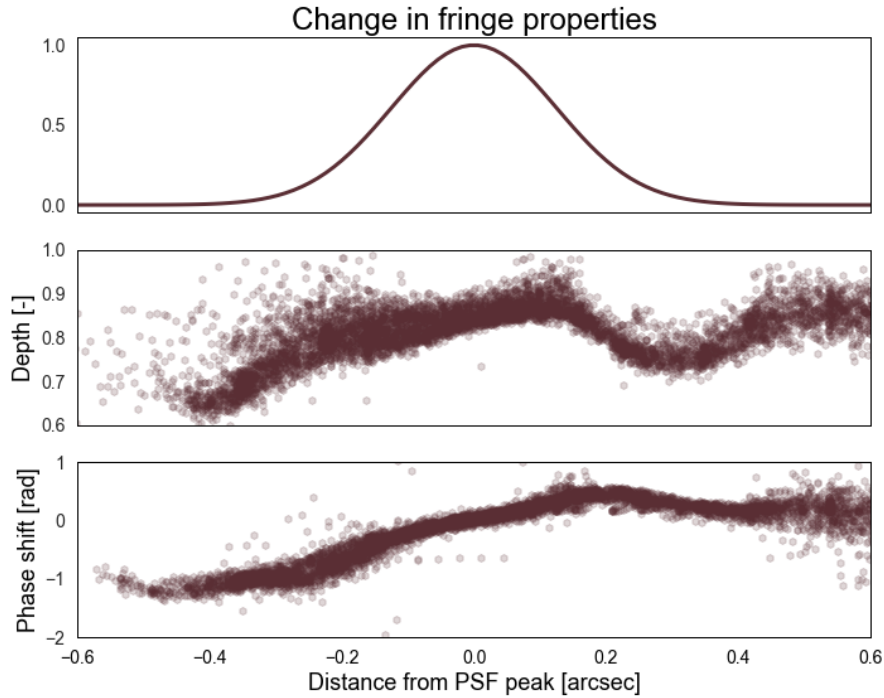


Figure 4. Fringe depth and phase as a function of distance from the PSF. A clear trend can be observed in both. Table 2. Priors for the Bayesian fitting loop. The lower and upper limits are the same for both the first and second body, except for the relative illumination, where the second body is assumed to be a fraction of the first.

Parameter	Lower limit	Upper limit
α	0.859 [arcsec]	1.459 [arcsec]
β	-0.454 [arcsec]	-0.254 [arcsec]
I	0.333 (1 for first body)	1

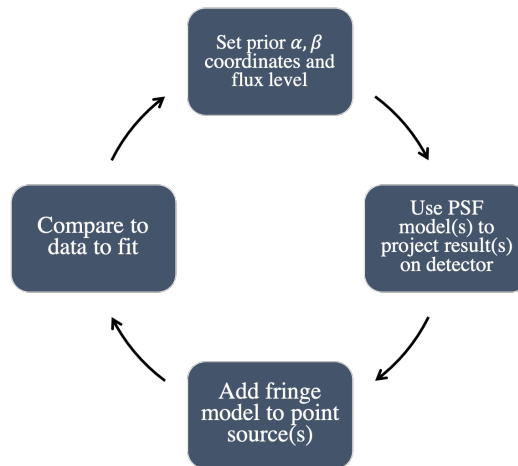


Figure 5. Schematic showing the Bayesian fitting loop.

3. RESULTS

Both the single- and two-body set-ups were run for 48 hours on a cluster. The results can be found in Fig. 6. While the centroids in α converge, this is not yet the case for β or the relative brightness. The pattern of the

fringes seems less dependent on these properties, making it more difficult to determine their values. Finding a more accurate fringe model, and potentially including information from other channels, could help constrain these parameters further.

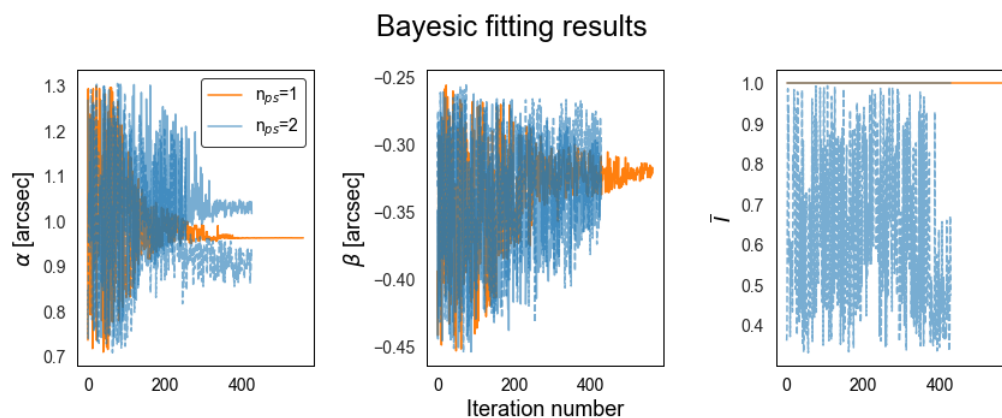


Figure 6. Results of the Bayesian fitting loop. It is able to converge to the correct centroid in the MRS along-slit direction (α). The fringes are not as sensitive to the sources' across-slit (β) position, hence convergence is not reached.

4. DISCUSSION

The results presented here focused on ground test data, and were therefore limited to band 1A. However, a variety of point sources were observed in all twelve bands in-flight. This allows us to take an initial look at how the point source fringes behave in other bands.

Firstly, due to the dependency of the fringe frequency on the wavelength, the period of the fringes increases for the longer wavelength channels when their origin remains the same. However, the reflective properties of the different detector layers change with wavelength as well. This means that in channels 2 and 3 an additional long-periodic component is introduced by reflections in the buried contact, and channel 4 is impacted by unresolved fringes due to the dichroics further upstream in the MRS optical path. These effects were known prior to launch, (**source**) and we have observed these in commissioning data as well.

Aside from changes due to the detector's properties, we can expect the asymmetric pupil illumination to have a similar effect on the fringes in the other channels. Indeed, this is the case for bands 2A through 3A, as presented in the smoothed fringe signals in Fig. 7. These were derived from the A-star observed during programme 1050 of commissioning. However, the larger background in the longer wavelengths seems to result in a more evenly illuminated detector, causing the fringes to be closer to those of an extended source, with little to no variability in depth and phase away from the PSF peak. However, these bands are low in flux and are affected by noise, hence the extent of this effect needs to be investigated further. This is beyond the scope of the current work.

Assuming that the change in fringe properties is significant up to at least band 3A, the method presented can be applied to the other bands as well. Especially since the observations per sub-band (A, B, or C) are taken simultaneously, it can be assumed that the on-sky coordinates are consistent and the data of two channels can be fit at once, provided the conversion to detector coordinates is sufficiently accurate.

5. CONCLUSIONS AND FUTURE WORK

While we are able to detect the presence of a nearby companion using the MRS fringe information in a Bayesian framework, work still needs to be done to improve the forward model in order to fit all parameters well. The fringes are more sensitive in the along-slit direction than the across-slit direction, causing the β -coordinate to be more difficult to find. Additionally, combining information from channels exposed simultaneously may improve the fit as well.

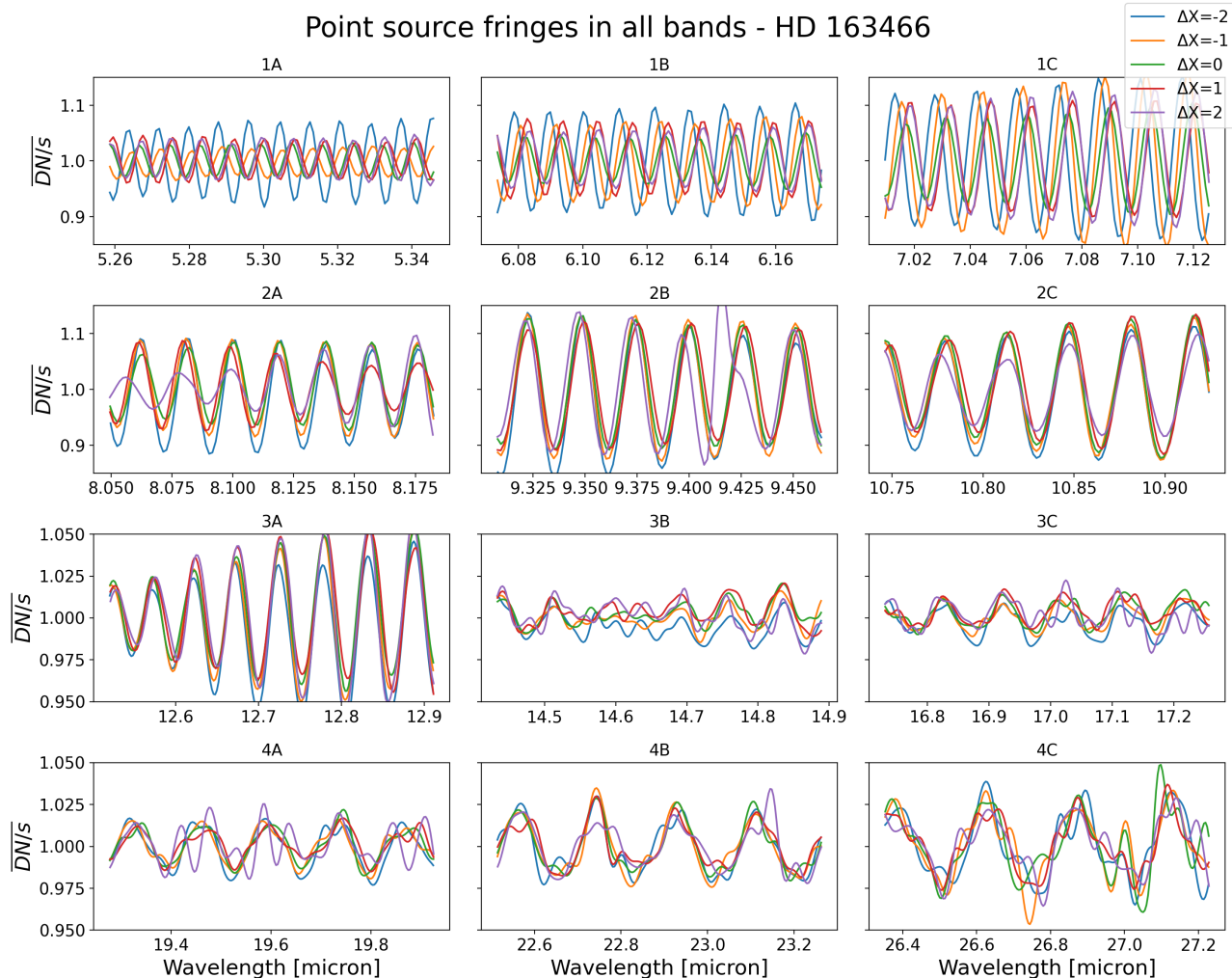


Figure 7. Normalised fringe signal per band, for the A-star HD 163466. A gaussian filter has been applied to all bands (2σ for channels 1 and 2, 3σ for channel 3, and 4σ for channel 4), to mitigate the effects of noise. In channel 4 a large part of the scatter, which is smoothed out, is due to the dichroic fringes.

In the work presented here, only two companions of similar flux were examined. However, by using simulated point source models and real observations we can test the limits in contrast and offset between companions, beyond which no evidence of additional sources can be found.

Once crowded fields can be examined using the framework presented here, we can extend the code to include other complex scenes, such as simulating disks by combining a set of point sources. By doing so, the scene at hand can be better characterised, and combining the spatial (PSF) and spectral (fringe) information will allow to extract MRS absolute fluxes in an optimal way.

ACKNOWLEDGMENTS

Danny Gasman, Ioannis Argyriou, and Bart Vandenbussche thank the European Space Agency (ESA) and the Belgian Federal Science Policy Office (BELSPO) for their support in the framework of the PRODEX Programme. The work presented is the effort of the entire MIRI team and the enthusiasm within the MIRI partnership is a significant factor in its success. MIRI draws on the scientific and technical expertise of the following organisations: Ames Research Center, USA; Airbus Defence and Space, UK; CEA-Irfu, Saclay, France; Centre

Spatial de Liège, Belgium; Consejo Superior de Investigaciones Científicas, Spain; Carl Zeiss Optronics, Germany; Chalmers University of Technology, Sweden; Danish Space Research Institute, Denmark; Dublin Institute for Advanced Studies, Ireland; European Space Agency, Netherlands; ETCA, Belgium; ETH Zurich, Switzerland; Goddard Space Flight Center, USA; Institute d’Astrophysique Spatiale, France; Instituto Nacional de Técnica Aeroespacial, Spain; Institute for Astronomy, Edinburgh, UK; Jet Propulsion Laboratory, USA; Laboratoire d’Astrophysique de Marseille (LAM), France; Leiden University, Netherlands; Lockheed Advanced Technology Center (USA); NOVA Opt-IR group at Dwingeloo, Netherlands; Northrop Grumman, USA; Max-Planck Institut für Astronomie (MPIA), Heidelberg, Germany; Laboratoire d’Etudes Spatiales et d’Instrumentation en Astrophysique (LESIA), France; Paul Scherrer Institut, Switzerland; Raytheon Vision Systems, USA; RUAG Aerospace, Switzerland; Rutherford Appleton Laboratory (RAL Space), UK; Space Telescope Science Institute, USA; Toegepast- Natuurwetenschappelijk Onderzoek (TNO-TPD), Netherlands; UK Astronomy Technology Centre, UK; University College London, UK; University of Amsterdam, Netherlands; University of Arizona, USA; University of Bern, Switzerland; University of Cardiff, UK; University of Cologne, Germany; University of Ghent; University of Groningen, Netherlands; University of Leicester, UK; University of Leuven, Belgium; University of Stockholm, Sweden; Utah State University, USA. A portion of this work was carried out at the Jet Propulsion Laboratory, California Institute of Technology, under a contract with the National Aeronautics and Space Administration.

We would like to thank the following National and International Funding Agencies for their support of the MIRI development: NASA; ESA; Belgian Science Policy Office; Centre Nationale D’Etudes Spatiales (CNES); Danish National Space Centre; Deutsches Zentrum für Luft-und Raumfahrt (DLR); Enterprise Ireland; Ministerio De Economía y Competividad; Netherlands Research School for Astronomy (NOVA); Netherlands Organisation for Scientific Research (NWO); Science and Technology Facilities Council; Swiss Space Office; Swedish National Space Board; UK Space Agency.

We take this opportunity to thank the ESA JWST Project team and the NASA Goddard ISIM team for their capable technical support in the development of MIRI, its delivery and successful integration.

REFERENCES

- [1] Wells, M., Pel, J. W., Glasse, A., Wright, G. S., Aitink-Kroes, G., Azzollini, R., Beard, S., Brandl, B. R., Gallie, A., Geers, V. C., Glauser, A. M., Hastings, P., Henning, T., Jager, R., Justtanont, K., Kruizinga, B., Lahuis, F., Lee, D., Martínez-Delgado, I., Martínez-Galarza, J. R., Meijers, M., Morrison, J. E., Müller, F., Nakos, T., O’Sullivan, B., Oudenhuisen, A., Parr-Burman, P., Pauwels, E., Rohloff, R. R., Schmalzl, E., Sykes, J., Thelen, M. P., van Dishoeck, E. F., Vandenbussche, B., Venema, L. B., Visser, H., Waters, L. B. F. M., and Wright, D., “The Mid-Infrared Instrument for the James Webb Space Telescope, VI: The Medium Resolution Spectrometer,” *PASP* **127**(953), 646 (2015).
- [2] Malumuth, E. M., Hill, R. S., Ted Gull, B. E. W., Bowers, C. W., Kimble, R. A., Lindler, D., Plait, P., and Blouke, M., “Removing the Fringes from Space Telescope Imaging Spectrograph Slitless Spectra,” *PASP* **115**(804), 218–234 (2003).
- [3] Argyriou, I., Wells, M., Glasse, A., Lee, D., Royer, P., Vandenbussche, B., Malumuth, E., Glauser, A., Kavanagh, P. J., Labiano, A., Lahuis, F., Mueller, M., and Patapis, P., “The nature of point source fringes in mid-infrared spectra acquired with the James Webb Space Telescope,” *A&A* **640**, A150 (2020).
- [4] Bailén, F. J., Suárez, D. O., and del Toro Iniesta, J. C., “On Fabry-Pérot Etalon-based Instruments. I. The Isotropic Case,” *ApJS* **241**(1) (2020).
- [5] Trotta, R., “Bayes in the sky: Bayesian inference and model selection in cosmology,” *Contemp Phys* **49**(2), 71–104 (2008).
- [6] Kester, D. J. M., Beintema, D. A., and Lutz, D., “SWS Fringes and Models,” in [*The Calibration Legacy of the ISO Mission*], Metcalfe, L., Salama, A., Peschke, S. B., and Kessler, M. F., eds., *ESA Special Publication* **481**, 375 (Jan. 2003).
- [7] <https://jwst-pipeline.readthedocs.io/en/latest/>.
- [8] Born, M. and Wolf, E., [*Principles of Optics*] (1999).
- [9] Kester, D. and Mueller, M., “BayesFit, a PYTHON Toolbox for Bayesian Fitting and Evidence Calculation,” *Astron. Comput.* **37** (2021).